AADE-03-NTCE-51

The Effects of Bit Nozzle Geometry on the Performance of Drill Bits

Dr. Michael R. Wells, PLUERE Inc., Rolf C. Pessier, Hughes/Christensen

Abstract

In recent years, a number of new nozzle designs have been proposed to the oil industry. These designs were developed to enhance turbulence, or reduce bottom hole pressure thereby improving the rate of penetration of roller cone and PDC bits.

Seven commercially available nozzles have been analyzed then compared to a conventional round nozzle. The analysis focused on the details of the flow field, velocity and pressure distributions, turbulence levels, and the impingement footprint. In addition, laboratory drill tests and field evaluations of some of these nozzles were reviewed. The results of the numerical analysis indicate that variations in nozzle exit shapes did not appreciably alter the jet flow from that of a conventional round jet. Nor was any improvement in drilling efficiency found in any of the laboratory or field tests. Nozzles that alter the direction of the jet or introduce swirl could be useful to clean the center of the drill bit or other difficult to access areas.

Introduction

Over the past several decades, numerous attempts have been made to improve the efficiency of the drilling process by optimizing the hydraulics beneath the bit.[1,2,3,4] Most efforts have either focused on the number and size of bit nozzles and nozzle alignment or on the specific geometry of the nozzle itself. It is well known that changes to the nozzle profile and exit geometry can produce sizable changes in the flow structure of the resulting turbulent jet.[5,6] These changes include, but are not limited to, the scale and intensity of the turbulence, the jet spreading characteristics and the virtual origin of a turbulent jet.[5,6] Some investigators have attempted to capitalize on large scale pressure fluctuations or cavitation generated by internal nozzle geometry to specifically improve drilling efficiency.[7,8]

Typically, nozzle configurations are designed to promote one or all of four primary flow properties in the jet. These are 1) high velocity, 2) impingement pressure, 3) high turbulence levels and 4) high jet spread to influence a large area at impingement. The intended application has a large bearing on which flow features are exploited. For roller cone bit applications, for example, high bottom hole shear, impingement velocity, is advantageous to aid in bottom hole cleaning along with high jet spread to increase the area along the hole bottom directly influenced by the jet. Moderate to high shear adjacent to the cone, sufficient to clean without causing severe erosion, can also reduce balling on the cones. High turbulence levels can aid in cleaning the bit and hole bottom by inducing negative pressure fluctuations at the surfaces and improving dispersion of the loose cuttings material in the flow. Nozzles intended for use in PDC bit applications are typically designed to generate wide, high velocity jets to help push cuttings through the junk slots and cool the cutters. In PDC applications, turbulence is secondary in importance to velocity.

Recently, several new nozzle designs have been introduced to the drilling industry.[9-18] These designs alter the jet flow from that produced by conventional "round" bit nozzles through either changes to the nozzle exit shape or in the internal geometry of the nozzle. The goal of this study was to numerically analyze the flow produced by seven of the unique nozzles found in the literature, and to identify flow features that might lead to improved bit and bottom hole cleaning. In concert with the numerical study were drilling experiments and field tests to correlate ROP improvements with identifiable flow enhancements brought about by nozzle design.

Numerical Technique

The numerical calculations were performed using a commercially available finite volume computer code, FLUENT. The basic equations of fluids in motion, Navier-Stokes equations, were solved iteratively to

obtain a steady state solution. Numerical convergence was confirmed when the normalized residuals of each solved equation were reduced by four orders of magnitude. The turbulence was modeled using a full Reynolds stress model that solves transport equations to resolve the Reynolds stresses in the time averaged momentum equations. Calculations were also made using the well established k-ε turbulence model for comparison. The fluid used in the simulations was water, at 80 °F in every case. The size of the computation mesh was purposely kept large to resolve the fine details in the flow. The mesh size varied with nozzle geometry but ranged from 500,000 to 1,200,000 cells. The mesh was then adapted periodically, adding 50-100k cells in regions of high velocity gradient to improve the accuracy of the solution.

A schematic of the simulation test apparatus is shown in Fig. 1, which also serves to define the nomenclature. Flow was supplied to the nozzles through a 0.88 inch diameter cylindrical tube. The velocity and turbulence values at the inlet corresponded to fully developed turbulent flow for the given inlet diameter. The flow rate through each nozzle was adjusted to maintain a Reynolds number (Re), based on the nozzle exit diameter, of approximately 760,000. The jets generated by the nozzles were submerged in a 12 inch diameter cylindrical tank and impinged vertically on the flat bottom. All nozzles were sized to have an equivalent exit diameter of 13/32 inch, based on the nozzle exit area. The nozzle standoff was set to be ten nozzle diameters, or 4.0625 inches, from the impingement point. The pressure along the exit plane at the top of the tank was assumed to be constant at 100 psi.

Numerical Verification

Simulations were performed using a standard, circular, bit nozzle to assess the accuracy of the numerical technique and to supply base data with which to compare the test nozzles against. The flow generated by a symmetric circular nozzle, having internal contours typical of those found standard in the drilling industry, was used as a baseline for comparison, Fig. 2.

The results of the simulations are compared to experimental data[19] and with data found in the open literature[20-25] in Figs. 3-8. A comparison was made of the key flow features listed above. Contours of the jet velocity are also shown in Fig. 3, which illustrates the jet spread, and the approximate length of the potential core region. The figures indicate that the velocity distribution, jet spread rate, axial distribution of turbulence and impingement pressure profile compare well with the experimental data. The impingement pressure distribution, Fig. 8, closely follows the typical Gaussian shaped distribution measured experimentally. In the remaining text, an impingement footprint is defined as twice the radial pressure half radius, β_p, as illustrated in the figure.

Nozzle Geometry

The seven nozzle designs used in this study are listed in Table 1. Each is commercially available and marketed to the oil industry[9-18]. Some of these designs are intended for use in PDC drill bits while others may be more focused on roller cone bit applications. In most cases the nozzle geometry used in the simulations is derived from published data or appropriate patent applications. The geometry, therefore, could be slightly different than that used in production nozzles.

The nozzles tested are divided into three categories. The first group consists of nozzle designs that alter the exit geometry while leaving the internal contours similar to typical, round, bit nozzles. The second group, containing only one nozzle, generates a jet flow exiting at an angle from the nozzle axis providing directional capability. Finally, the third group consists of nozzles that generate swirl flows or swirling jets aimed to increase the jet spread.

Exit Geometry Designs

Star Nozzle[9,10,11]

The geometry of the star nozzle used in the simulations is illustrated in Fig. 9. This design is characterized by a six-vane star shaped exit geometry. The internal contours leading to the star exit are essentially the same as the round nozzle. The vanes making up the star points act as shear stress risers forcing flow to the center of the star, slightly reducing the effective nozzle diameter. This increases the flow in the center of the jet by approximately 6 ft/sec over the round jet and proportionally reduces the jet diameter, see Fig. 20. The small size of the vanes promotes high mixing, tending to rapidly remove any traces of the exit geometry from the flow. The star shape remains evident in the flow velocity for only approximately one nozzle diameter from the exit, at which point the jet resumes the appearance of the typical round nozzle.

Slot, Y and Cross Nozzles[12,13]

Similar to the Star Nozzle, the Slot, Y and Cross nozzle are characterized by two, three and four vanes at the nozzle exit, Figs. 10,11,12. The internal nozzle contours of the Slot, Y and Cross nozzle are essentially cylindrical with a conical shaped exit[13]. The exit geometry is designed to increase turbulence to provide superior bit

cleaning while generating negative pressure at the hole bottom to create an underbalance environment near the cutting structure. Like the Star nozzle, however, the resulting flow rapidly degenerates into a flow structure similar to the round jet, where within 2 nozzle diameters the contours of velocity become circular. The simulations show, however, that as the number of vanes decreases, the departure of the flow from a typical circular jet increases. For example, the Slot and Y nozzles, having two and three vanes respectively both exhibit slightly higher jet spread characteristics, and consequently lower axial velocities, than the others in the exit geometry category, see Figs. 24 and 20 respectively.

Directional Nozzle

Fluted Nozzle[12,13,14]

The Fluted Nozzle is designed so that the nozzle exit is slightly off center. On one side, the internal nozzle contour is linear, projecting straight out from the base of the inlet. The opposite side is slightly built up with a "Fluted" structure, Fig. 13, which forces fluid radially outward, around the flute then back to cross jet axis, tilting the axis of the jet by approximately 11 degrees, Fig. 14. The design makes it possible to direct the jet in a bit to improve cleaning. The direction capability of the jet, however, also requires that the nozzle be properly orientated in the bit to optimize the hydraulics. At the nozzle exit, where the fluid from the Flute crosses the main stream of the jet, the magnitude of velocity is slightly higher than the typical circular nozzle, but the component of velocity along the jet axis is nearly the same. Along the axis, the flow regime is very similar to the round jet.

The results presented below for the Fluted nozzle have been corrected to account for the approximate 11 degree tilt of the jet. This displacement also makes the actual standoff of the Fluted nozzle, the distance from the nozzle exit to the impingement point along the jet axis, slightly longer than would be the case in a true vertical impingement.

Swirl Flow Designs

Dual-Jet Nozzle[15,16,17]

The "Dual-Jet" nozzle is designed to promote a swirling flow rotating about the jet axis. As the name suggests, the Dual-Jet nozzle is built around two distinct flow paths, shown schematically in Fig. 15. The inner path consists of a funnel shaped section that ports flow directly through the center of the nozzle, Fig. 16. The outer path is a vane section, imparting swirl to the flow in an annular region between the inner funnel and the outer housing, Fig. 17. The two flow paths then recombine within the nozzle in the "flow collection region", just prior to exiting.

The results of the simulations of the Dual-Jet nozzle show that the jet has only a small swirl component remaining once the flow exits the nozzle. Since the dual inlet to the nozzle sees the same absolute pressure, the significantly higher pressure loss associated with the swirl flow generation region inside the nozzle severely restricts the volume of the flow passing through this section. With the flow in the swirl section restricted, the component of the flow passing through the center of the nozzle dominates resulting in a turbulent jet that is very similar to that produced by a circular nozzle.

K-Nozzle[18]

The K nozzle is also designed to introduce a swirl component to the flow. With this design, fluid enters the nozzle through six inlet ports, Fig. 18. The inlet ports are positioned so that the flow enters at an oblique angle from the jet axis, imparting a swirl velocity to the flow. The swirling flow then passes through a cylindrical section before exiting. The swirl component of the flow significantly increases the jet spread rate, which broadens the zone of influence upon impingement, Fig. 19, at the expense of the jet axial velocity. The swirl also reduces the pressure along the axis of the jet, particularly at the point of impingement, since most of the energy is focused in the swirling region, see Table 1.

Nozzle Comparisons

The results of the simulations are grouped with respect to the three design categories; exit geometry, directional and swirl. The directional nozzle results are grouped with the swirl nozzles. Presented here are those characteristics that are believed to most likely to influence the rate of penetration of drill bits.

Discharge coefficient

The discharge coefficient is an indicator of the pressure required to supply a given flow rate through a nozzle. The value traditionally assumed for the pressure coefficient for a typical bit nozzle is 0.95, roughly corresponding to that documented for square orifices. Experimental evidence[20], however, suggests that a value of 1.03 is more appropriate for bit nozzles, suggesting that bit nozzles behave more like a venturi than an orifice. Table 1 lists the computed discharge coefficients for all nozzles. The table shows that while most nozzles have discharge coefficients very near that of the circular nozzle, the Slot and Y nozzles require 25% more

pressure to sustain a particular flow rate and the Dual-Jet requires over 120% more pressure.

TABLE 1 – Nozzle Results

Nozzle	Nozzle Discharge Coefficient	Impingement Footprint (in)	Imp. Pressure Max. (P_{imp} / ΔP_n)
Round	1.03	1.70	0.51
Star	1.00	1.49	0.55
Slot	0.92	2.11	0.15
Y	0.88	1.90	0.15
Cross	0.95	1.89	0.25
Fluted	1.02	1.65	0.57
Dual-Jet	0.69	1.92	0.17
K-nozzle	0.87	5.84	0.01

Axial Velocity Decay

The jet axial velocity imparts an impact force on the impingement surface that can greatly enhance cleaning. The decay of axial (centerline) velocity for the seven nozzles tested is shown in Figs. 20 and 21. Fig. 20 shows the results for the "nozzle exit geometry" group. The figure shows that the Slot and Y nozzles exhibit an abbreviated core region where the centerline velocity drops off at approximately 4 nozzle diameters from the exit while the other nozzles closely follow the circular jet with a potential core length of approximately 6.0 equivalent nozzle diameters. The length of the potential core regions of the Slot and Y nozzles appear to scale with the narrower width of their respective nozzle exits rather than the equivalent nozzle diameters. The rapid fall off of axial velocity in these two nozzles suggests that less energy would reach either the hole bottom or bit surfaces to improve cleaning. Fig. 21 shows a similar plot for the swirl nozzle group. Both the Dual-Jet and the Fluted nozzle follow the axial velocity decay of the standard circular bit nozzle. The K-nozzle, however, exhibits a rapid velocity decay along the centerline of the jet. Most of the energy of the K-nozzle is directed into the establishment of the swirl velocity that almost immediately spreads away from the jet axis, dramatically lowering the axial velocity component.

Axial Turbulent Kinetic Energy Distribution

The level of turbulence that a jet produces is an indication of the amount of lifting force available to remove cuttings at the bit surface and the hole bottom[1]. Turbulence also increases the level of flow induced dispersion the cuttings experience which would also aid in their removal from beneath the bit. Fig. 7 shows a comparison between experimental and predicted turbulence intensity for the circular nozzle. The turbulence intensity in this plot is made dimensionless with the axial mean velocity. The mean velocity along the jet axis varies widely between nozzle designs, thus influencing the value of the turbulence intensity. Therefore, a more direct measure of the turbulence level would be the computed turbulent kinetic energy. The turbulent kinetic energy is defined as the root mean square of the three components of fluctuating turbulent velocity. Figs. 22 and 23 show the distribution of axial turbulent kinetic energy for the two nozzle groups. Fig. 22 shows the turbulence generated by the exit geometry design group. The figure illustrates that the Slot and Y nozzles generate higher levels of turbulent energy near the nozzle exit than the circular nozzle while the other nozzles in this group generate approximately the same level of turbulence as the circular nozzle. The higher turbulent energy produced by the Slot and Y nozzles accounts, to some extent, for the rapid dispersion of axial velocity seen with these nozzles. The nozzles in the swirl group tend to generate slightly less axial turbulence than the circular nozzle, Fig. 23. This is particularly true of the K-nozzle, what appears to be relatively quiescent along the centerline of the jet.

Jet Spread Rate

Fig. 24 shows the jet spread rate produced by the various nozzle shapes. The jet spread rate is computed from the jet half distance, β, which is the radial distance where the jet velocity drops to half the centerline velocity. The jet spread rate is a measure of the increase in cross sectional area of the jet normal to the jet axis. Calculations to determine the jet spread rate were made in both coordinate directions perpendicular to the jet axis. Since all the nozzles generated a near circular flow pattern about the axis, the values obtained from each axial direction were, in every case, nearly identical. The spread rate computed for the Fluted nozzle was corrected for the tilt of the jet axis. All of the nozzles tested, except the K-nozzle, produced comparable jet spread rates. The Slot and Y nozzles produced jets with slightly higher spread rates than the circular nozzle, but this difference is small. The cross sectional area of the K nozzle was over four times that of a conventional nozzle at ten diameters from the exit.

Impingement Footprint

The impingement footprint is a measure of the size of the zone of influence along the impingement surface beneath the jet. This zone is analogous to the area at the bottom of the hole directly influenced by the jet flow. The footprint is defined as twice the radial distance along the impingement surface, from the impingement point, where the static pressure is half that at the point of impingement at the jet axis. Fig. 25 shows the distribution of the impingement footprints for all nozzles tested. The figure shows that all of the nozzles, except the K-nozzle, generate approximately the same size footprint. The calculated footprint of the K-nozzle is over three times the size of that generated by the circular nozzle. This larger area of influence is due to the high swirl velocity induced in the jet, forcing the flow to migrate radially outward.

Drill Tests

Drill tests and field evaluations using some of the nozzles tested were correlated with the numerical results in an attempt to isolate flow features that might have an influence on drill bit performance. The simulations show, however, that many of the nozzles displayed very similar flow characteristics so drill tests were selected to provide examples within the three primary design groups. The nozzles evaluated in the drill tests were the Star nozzle, the Dual-Jet nozzle and the Fluted nozzle.

The first drilling results are those using the Star nozzle. Figs. 26 and 27 show the results of two sets of highly controlled drilling experiments performed using a drilling simulator. The drilling simulator tests used two rock types, Berea Sandstone and Catoosa shale and a 6-1/4 inch PDC bit. Both sets of tests were performed with 4000 psi bottom hole pressure and 5 ksi WOB. Tests were first conducted using standard bit nozzles and then repeated using Star nozzles under similar conditions. The figures show that in both sets of tests, the Star nozzles made no apparent difference in ROP. Fig. 28 shows the results from a suite of field tests comparing the Star nozzle with a conventional nozzle. These runs were made with a 6-1/8 inch PDC drill bit in similar formations under similar operating conditions and at similar depths. As with the drilling simulator results, no clear benefit of the Star nozzle is evident from the tests.

Drilling simulator tests using the Dual-Jet nozzle are shown in Fig. 29. These tests were performed using a two-cone roller cone bit in Catoosa Shale with a 9.6 ppg drilling mud and 4,500 psi bottom hole pressure. The WOB and RPM were held constant at 50 klbs and 120 rpm respectively. The results show that the Dual-Jet nozzle had no appreciable effect on the drilling efficiency of the bit.

Finally, a series of drilling simulator tests were performed using the Fluted nozzle in an 8-1/2 inch, PDC bit. The tests were conducted in Catoosa shale with a bottom hole pressure of 1800 psi. The results are shown in Fig. 30. The results show that the Fluted nozzle produced no apparent improvement in ROP.

No laboratory drilling data is available for the K-nozzle. However, the design is being used commercially as a center jet on roller cone bits. The axial velocity of a conventional nozzle is too high in the center jet position and frequently erodes the spear point of the cones. The swirl jet distributes the fluid over a much larger area effectively cleaning the center of the bit without harmful erosion.

Conclusions

A numerical study has been performed to examine the flow characteristics generated by seven commercially available bit nozzles. The results were compared to similar results obtained using a standard, circular bit nozzle. The study showed that only the K-nozzle generated a jet flow that was substantially different from a standard bit nozzle. This difference was primarily due to the inducement of a strong swirl component to the flow that caused the jet produced by the K-nozzle to be significantly wider than the standard bit nozzle. The following conclusions are made as a result of this study.

1. Small features built into the exit of a bit nozzle have little effect on the resulting jet. The size of the exit feature is limited by the small diameter of the nozzle body. The smallest features, as used by the Star and the Cross nozzles, tend to disappear in the flow after about one nozzle diameter from the nozzle exit. Larger features, as seen with the Slot and Y nozzles, persisted in the flow for longer distances from the exit, suggesting that features in the nozzle exit must be large in scale to affect the structure of the jet. The gross characteristics of these two jets, however, such as the potential core length, tended to scale with the slot widths rather than the equivalent nozzle diameter, dramatically reducing the axial velocity of the jet, and thereby the cleaning or scouring force at impingement.

2. The dominant flow feature exhibited by the Fluted nozzle is a redirection of the jet by approximately 11 degrees from the nozzle axis. This characteristic can be used to improve hydraulics in poor performing bits if the nozzle is properly placed in the bit. The characteristics of the flow, however, (other than the jet axis redirection) are nearly

identical to that of the standard "round" nozzle.

3. The swirl component of the flow induced by the Dual-Jet nozzle is predominately dissipated within the nozzle where the two jet components, the center axial jet and the outer swirl jet, were recombined. Only slight evidence of a swirl component of the flow can be identified at one nozzle distance from the exit.

4. The K-nozzle generates a strong swirl component to the jet flow that dominates the flow regime. The spread of the jet produced by the K-nozzle is over 4 times that generated by a standard round jet, suggesting that it might have the ability to clean a significantly larger surface area. Most of the energy of the K-nozzle is exhausted providing swirl. Therefore, the axial velocity K-nozzle is much lower than that generated by the standard nozzle possibly reducing its capacity for cleaning. The impingement pressure at the impingement point is reduced to near zero (neglecting the external static pressure) indicating that the actual impingement occurs at the outer region of the swirl flow regime.

5. The laboratory drill tests and field results are in agreement with the results from the simulations. The simulations show that the turbulent jets generated by the test nozzles differ only slightly from the standard nozzle. Correspondingly the laboratory drill tests and field results indicate no change in bit performance using the nozzles.

Acknowledgements

The author wishes to thank the personnel at Hughes/Christensen for their support in the completion of this study.

Nomenclature

A_o = nozzle area (in2)
D = bit diameter (in)
d_o = nozzle exit diameter (in)
H = nozzle standoff (in)
HSI = hydraulic horsepower per sq. in. of bit area.
K = nozzle discharge coefficient $K = V_o/SQRT(2\ \Delta P_n/\rho)$
k = turbulent kinetic energy
P = static pressure
P_{imp} = static pressure at the impingement point
P(r) = radial distribution of static pressure
P(z) = vertical, z, distribution of static pressure
ΔP_n = nozzle pressure drop
Q = flow rate (gpm)
r = radial distance from the jet axis (in)
ROP = rate of penetration (ft/hr)
RPM = bit rotary speed (rpm)
*TI = turbulence intensity based on the local mean velocity (%), TI = SQRT(2*k/3)/|V| = Vrms/|V|*
V_{cl} = axial jet velocity (ft/sec)
V_o = nozzle exit velocity (ft/sec)
|V| = local mean velocity
V_{rms} = root mean square turbulent velocity
WOB = weight on bit (kips)
z = coordinate direction beginning from the nozzle exit to the impingement plate (in)
ε = turbulent eddy dissipation
ρ = fluid density
ν = fluid dynamic viscosity (ft2/sec2)
β = the radial location where the velocity is equal to half the axial velocity (in)
β_p = the radial location where the pressure is equal to half the axial impingement pressure (in)

References

1. Wells, M. R.: "Dynamic Rock Chip Removal by Turbulent Jetting," SPE 14218, 1986
2. Wells, M. R., Pessier, R. C.: "The Effects of Asymmetric Nozzle Sizing on the Performance of Roller Cone Bits," SPE 25738, 1993
3. Cheatham, J. B. Jr., Yarbrough, S. G.: "Chip Removal by a Hydraulic Jet," Soc. Pet. Ing. J. Vol. 231, March 1964, Trans AIME, pp. 21-25
4. Ledgerwood, L. W., Wells, M. R., Wiesner, B. C., Harris, T. M.: "Advanced Hydraulic Analysis Optimizes Performance of Roller Cone Drill Bits,", IADC/SPE 59111, 2000
5. Wlezien, R. W., Kibens, V.: "Passive Control of Jets with Indeterminate Origins," AIAA Paper 84-2299, 1984
6. Husain, H. S., Jussain, A. K. M. F.: "Controlled Excitation of Elliptic Jets," Physics of Fluids, Vol. 26, October 1983, pp.2673-2765
7. Johnson, V. S. Jr., Chahine, G. L., Lindenmut, W. T., Conn, A. F., Frederick, G. S.: "The Development of Structured Cavitating Jets for Deep-Hole Bits," SPE 11060, 1982
8. Rongqing, L., Wu, J. Juvkam-Wold, H. C.: "New Nozzle to Increase Drilling Rate by Pulsating Jet Flow," IADC/SPE 27468, 1994
9. "The Lobestar Mixing Nozzle," Advertisement Brochure Vortex Ventures Inc.
10. Lott, W. G.: "Improved Nozzle Insert for Rotary Rock Bit," United States Patent No. 5,775,446
11. Lott, W. G.: "Improved Fluid Mixing Nozzle and Method", United States Patent No. 5,664,733

12. Dove, N. R., Smith, S. K., Lott, W. G.: “Vortex Drill Bit,” United States Patent No. 5,632,349
13. Dove, N. R., Smith, S. K., Lott, W. G.: “Vortex Method,” United States Patent No. 5,653,298
14. Akin, J. E., Dove, N. R., Smith, L. M.: “Fluted Nozzles Increase Penetration Rates, Extend Bit Life”, Oil & Gas J., May 10, 1999
15. “DualJet – The Power Inside” Prodril Services Inc. Operational Manual.
16. Curlett, Harry, B. “Method and Apparatus for Jet Cutting,” United States Patent No. 5,291,957, Mar. 8, 1994.
17. Curlett, Harry, B. “Method of an Apparatus for Jet Cutting,” United States Patent No. 5,199,512, April 6, 1993.
18. “Advantages of the Vortex Center Jet”, Hughes/Christensen Advertisement Bulletin
19. Unpublished experimental LDV measurements Amoco Production Research, 1985
20. Warren, T. M.: “Evaluation of Jet-Bit Pressure Losses,” SPE Drilling Engineering, Dec 1989, pp. 335 - 340
21. Giralt, F., Chia, C, Trass, O.: “Characterization of the Impinging Region in an Axisymmetric Turbulent Jet,” Ind. Eng. Chem Fundam., Vol 16, No. 1, 1977, pp. 21-28
22. Donaldson, C. D., Snedeker, R. S., Margolis, D. P.: “A Study of Free Jet Impingement. Part I. Mean Properties of Free and Impinging Jets,” JFM Vol. 45, part 2, 1971, pp. 281-319
23. Donaldson, C. D., Snedeker, R. S., Margolis, D. P.: “A Study of Free Jet Impingement. Part II. Free Jet Turbulent Structure and Impingement Heat Transfer,” JFM Vol. 45, part 3, 1971, pp. 477-512
24. Beltaos, S., Rajaratnam, N.: “Impinging Circular Turbulent Jets,” J. of the Hydraulics Division, ASCE, Vol. 100, No. HY10, Oct, 1974, pp. 1313-1328
25. Beltaos, S., Rajaratnam, N.: “Impingement of Axisymmetric Developing Jets,” J. of the Hydraulics Research, Vol. 15, No. 4, 1977, pp. 311-326
26. Independent tests performed at the Amoco Production Research Drilling Facility.

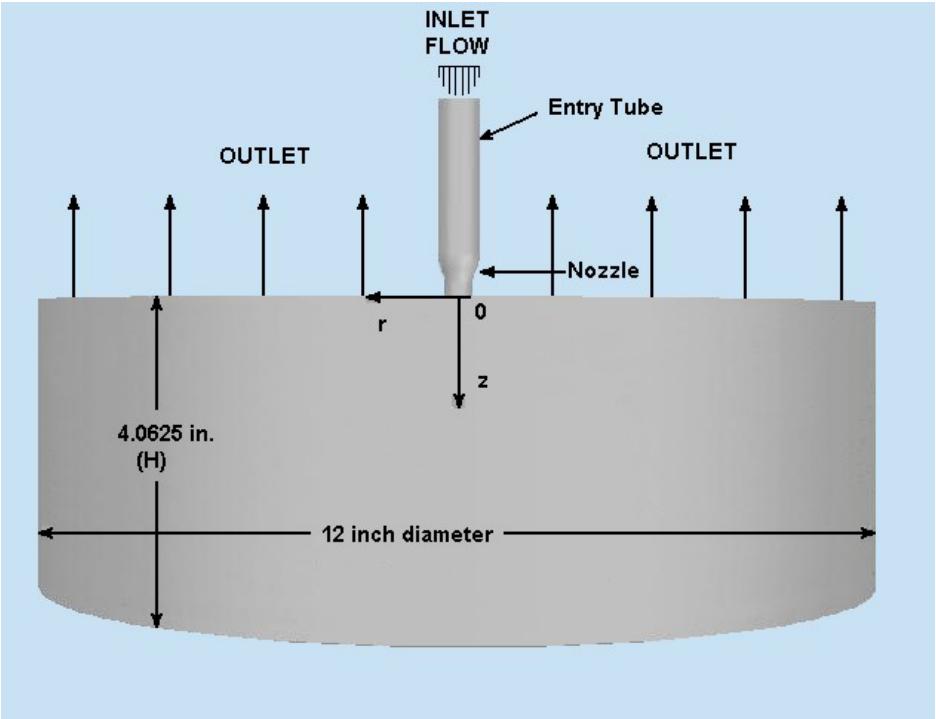

Figure 1 – Numerical Test Geometry

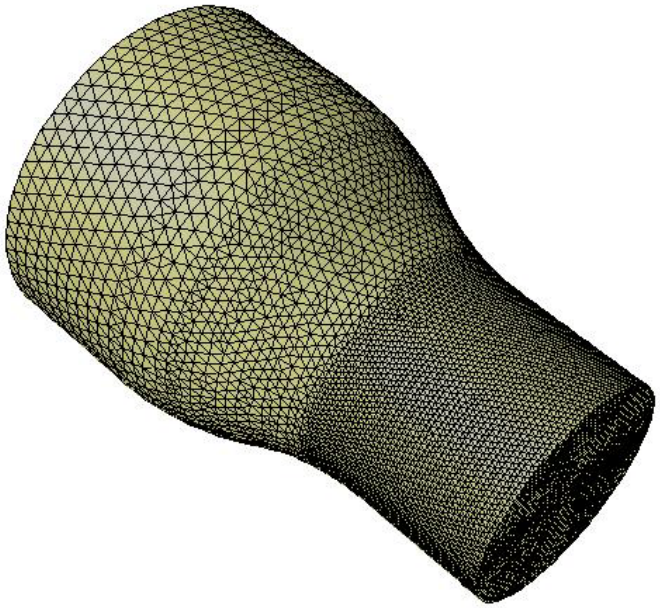

Figure 2 – Standard Circular Bit Nozzle

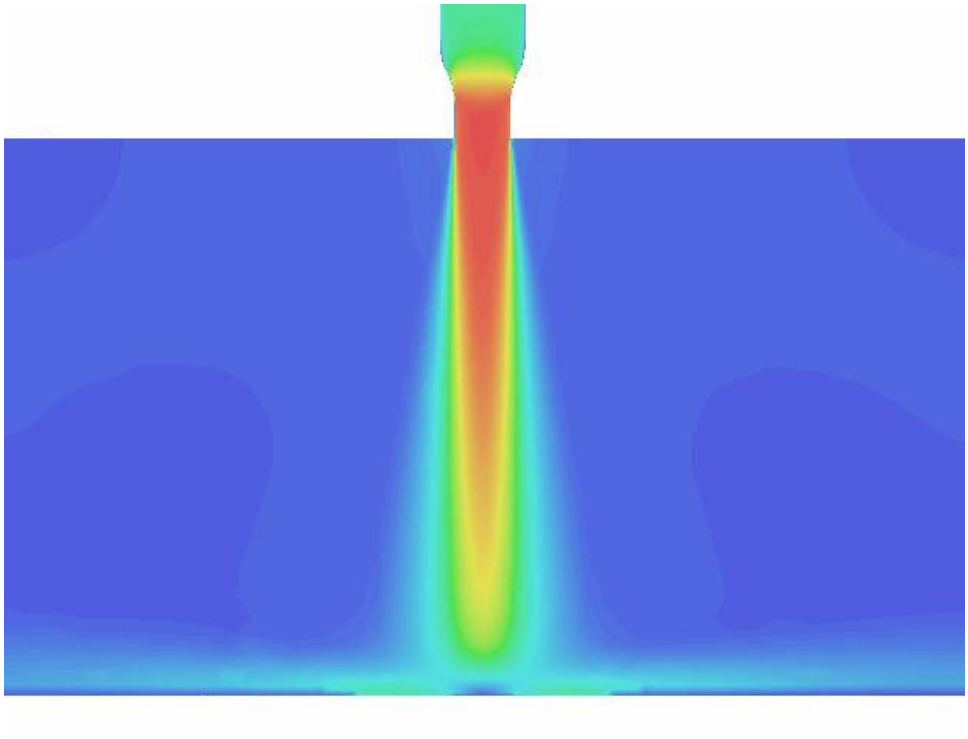

Figure 3 – Circular Jet Contours of Velocity Magnitude

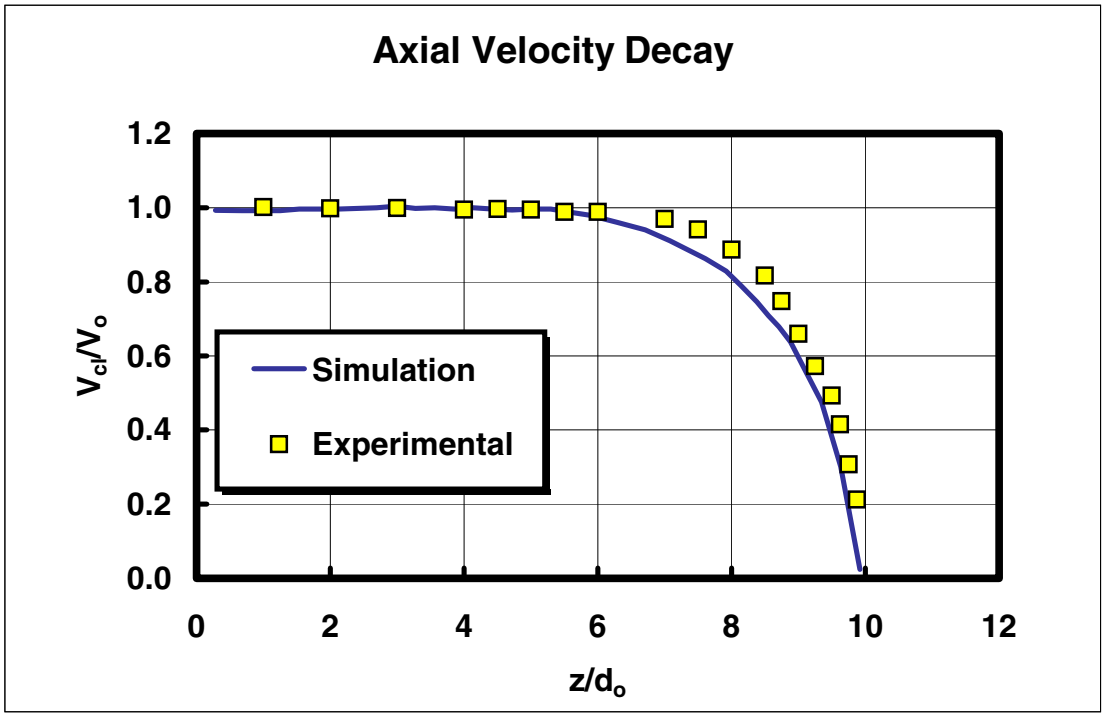

Figure 4 – Circular Jet Axial Velocity Decay

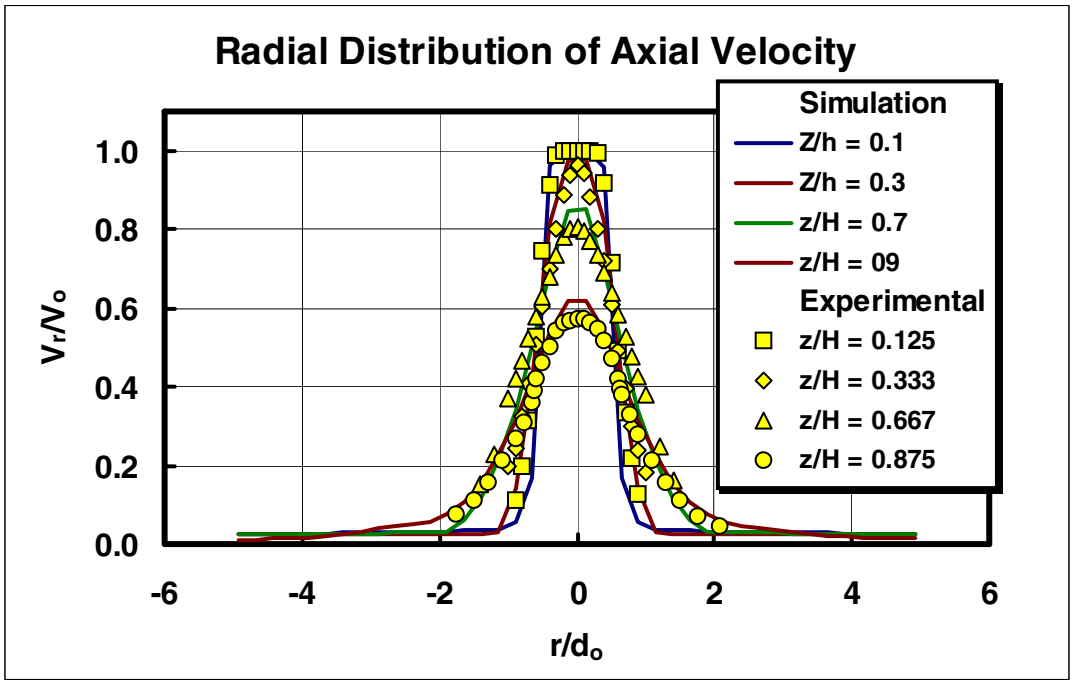

Figure 5 – Circular Jet Radial Velocity Distribution

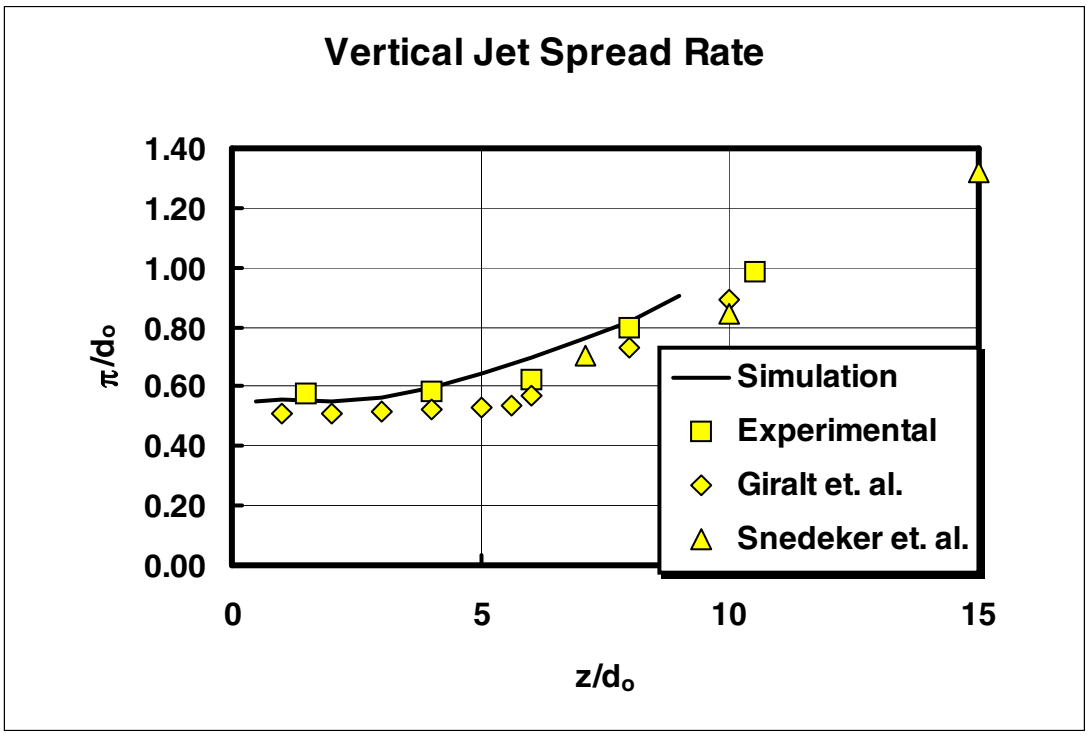

Figure 6 – Circular Jet Spread Rate

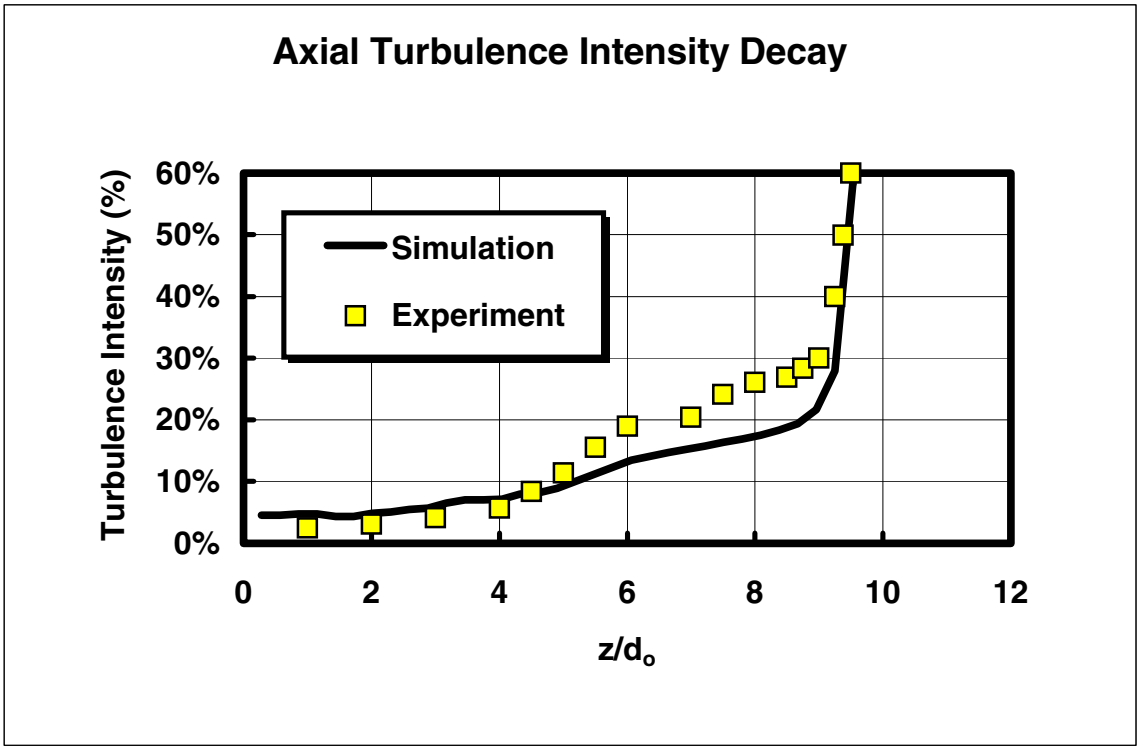

Figure 7 – Circular Jet Axial Turbulence Intensity Distribution

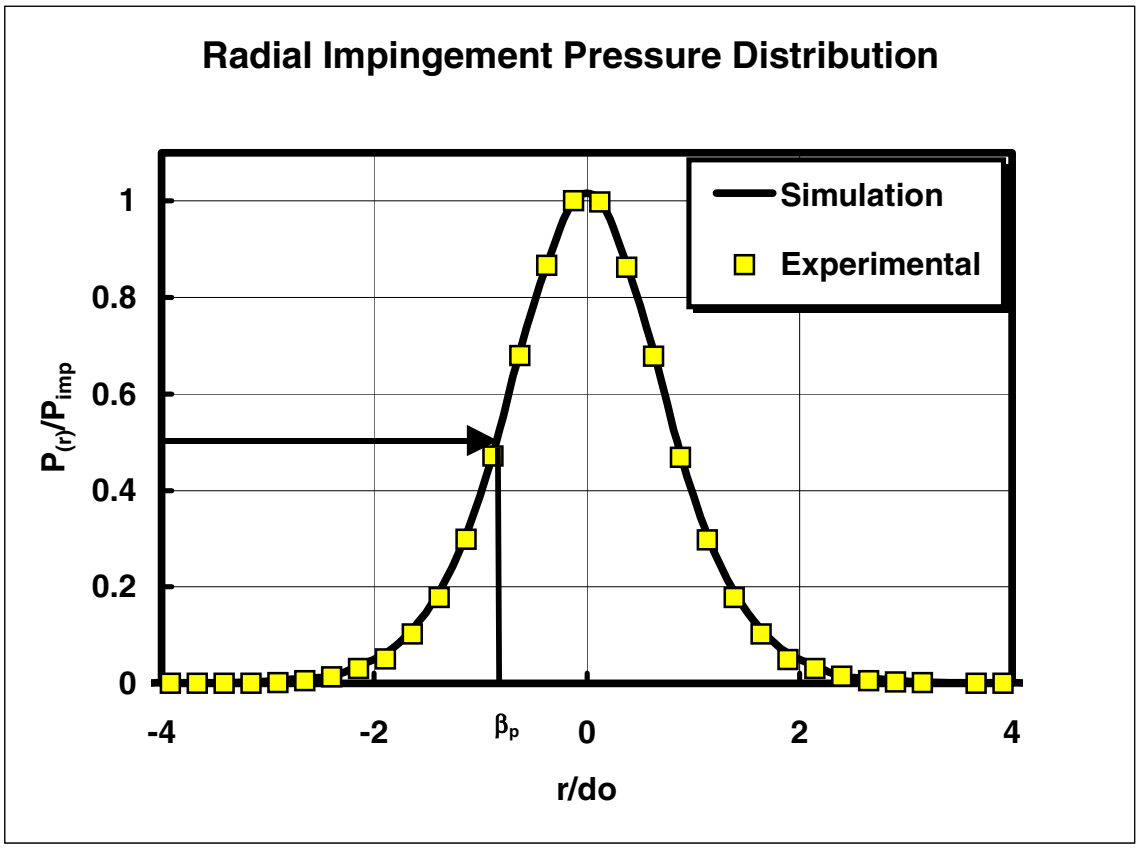

Figure 8 – Circular Jet Radial Impingement Pressure Distribution

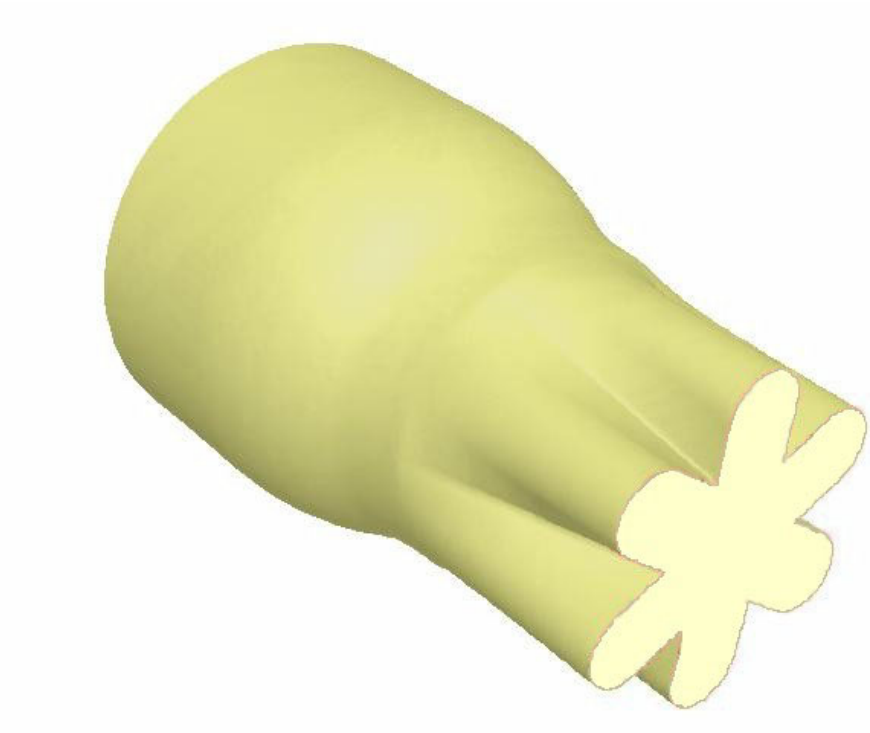

Figure 9 –Star Nozzle

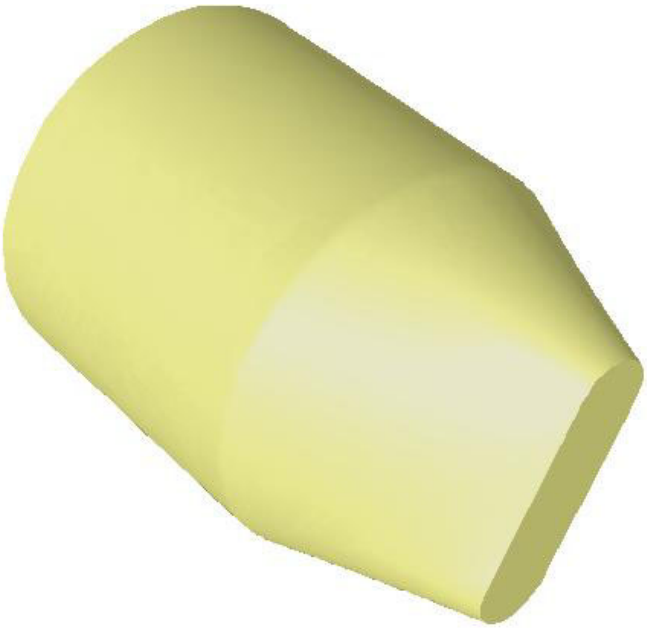

Figure 10 – Slot Nozzle

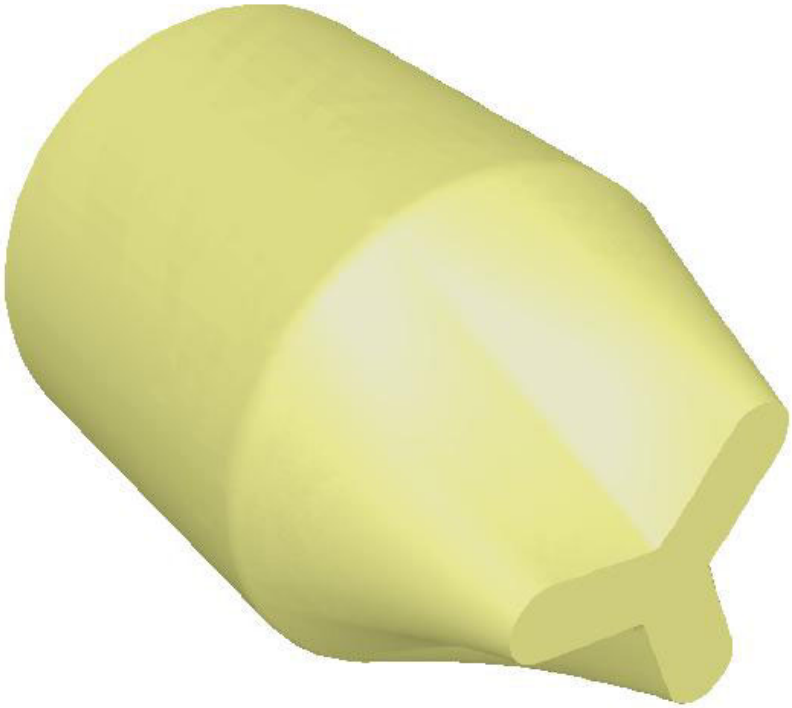

Figure 11 – Y Nozzle

Figure 12 – Cross Nozzle

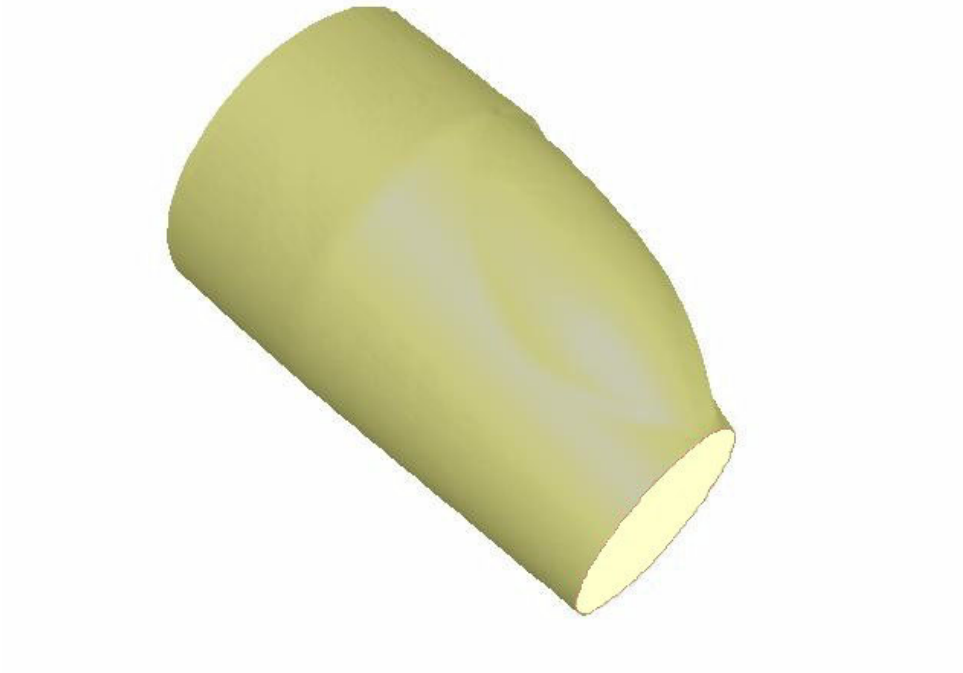

Figure 13 – Flute Nozzle

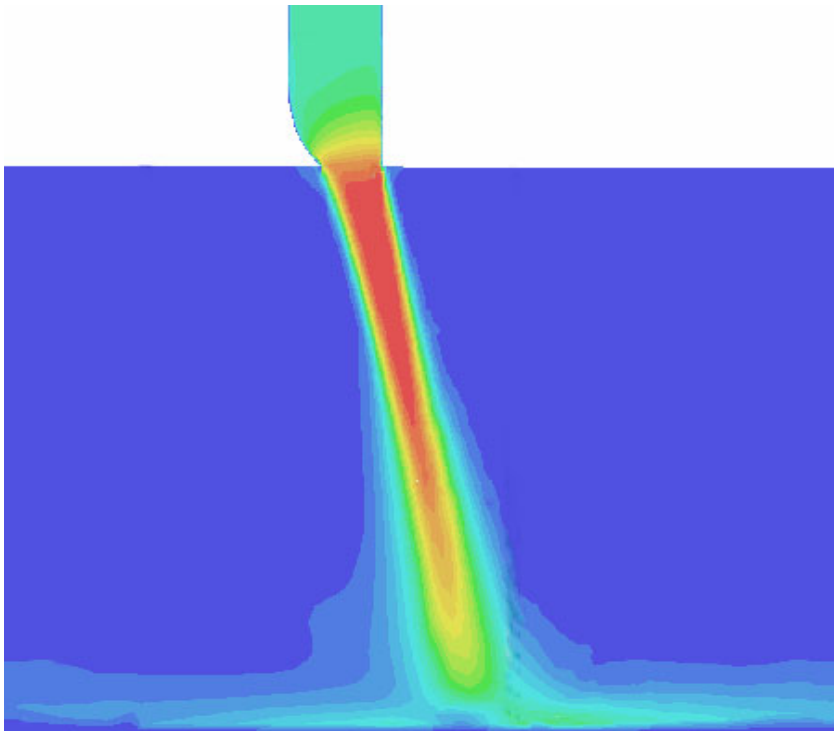

Figure 14 – Flute Nozzle Velocity Contours Showing Jet Axial Displacement

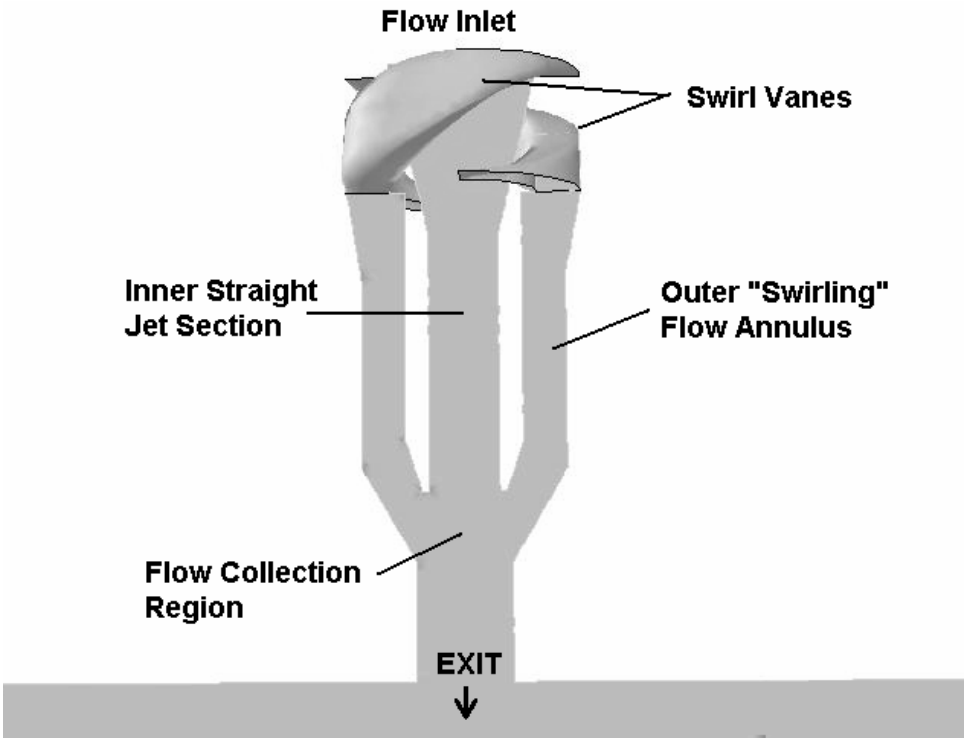

Figure 15 – Dual-Jet Nozzle Flow Schematic

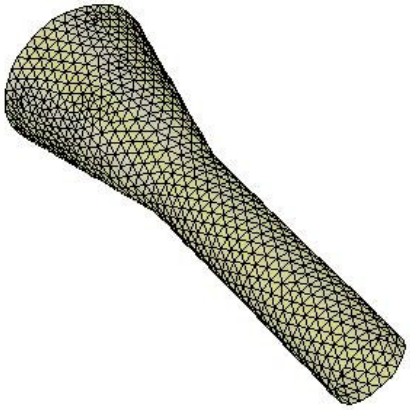

Figure 16 – Dual-Jet Inner Nozzle

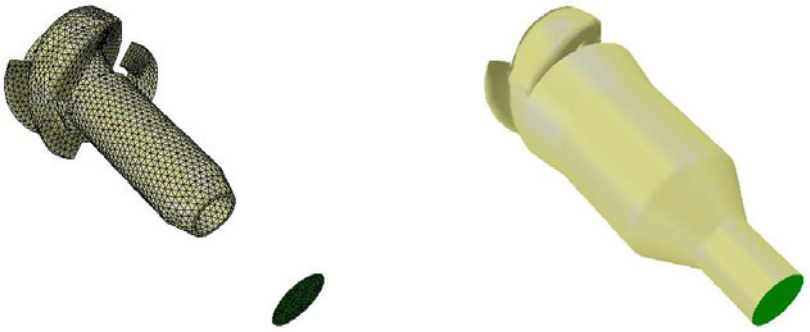

Figure 17 – Dual-Jet Outer Nozzle

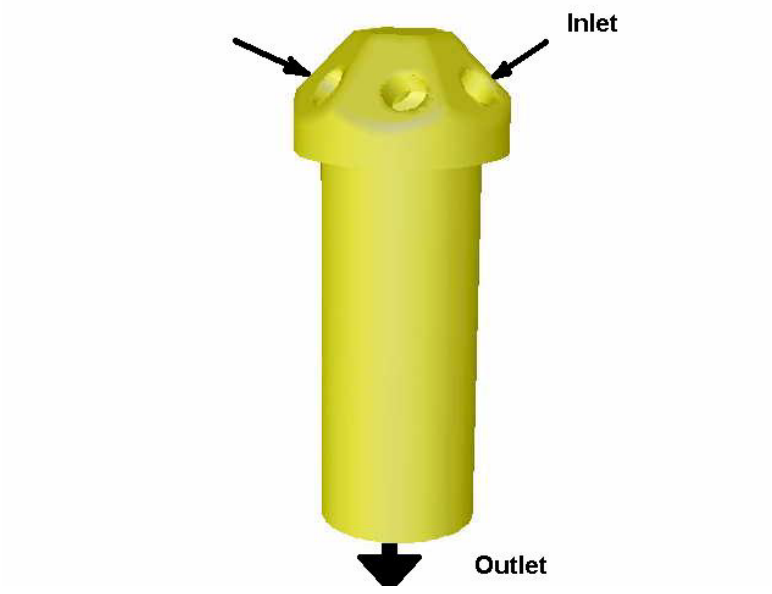

Figure 18 – K-nozzle

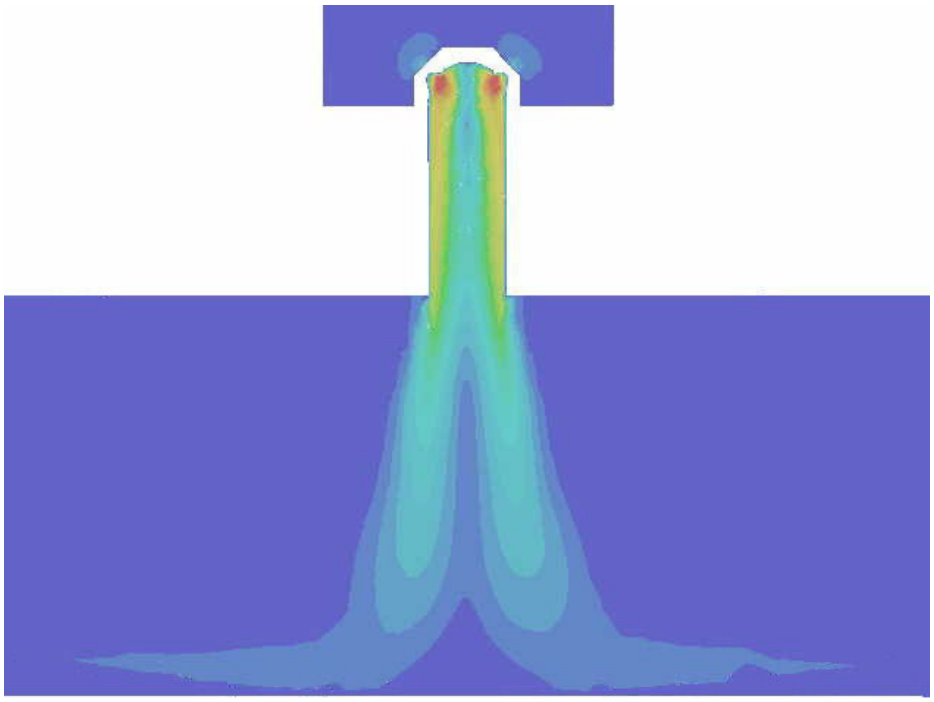

Figure 19 – K-nozzle Velocity Contours Showing Jet Spread Characteristics

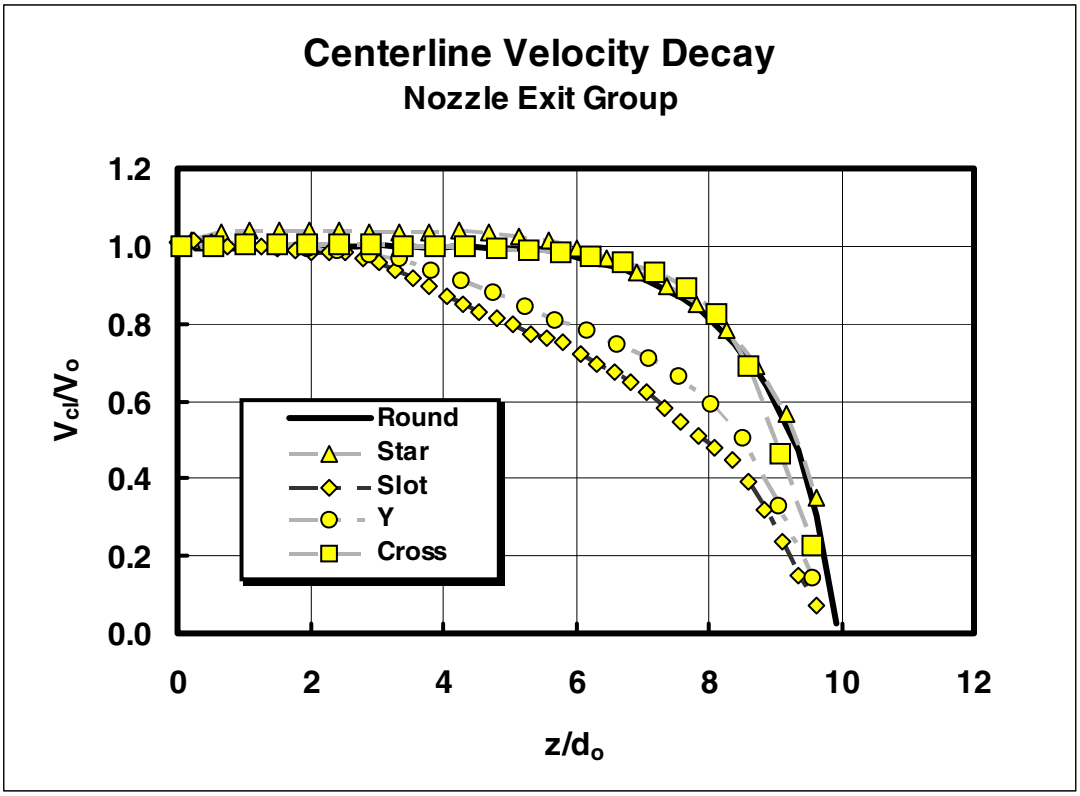

Figure 20 – Axial Velocity Decay – Exit Geometry Design Group

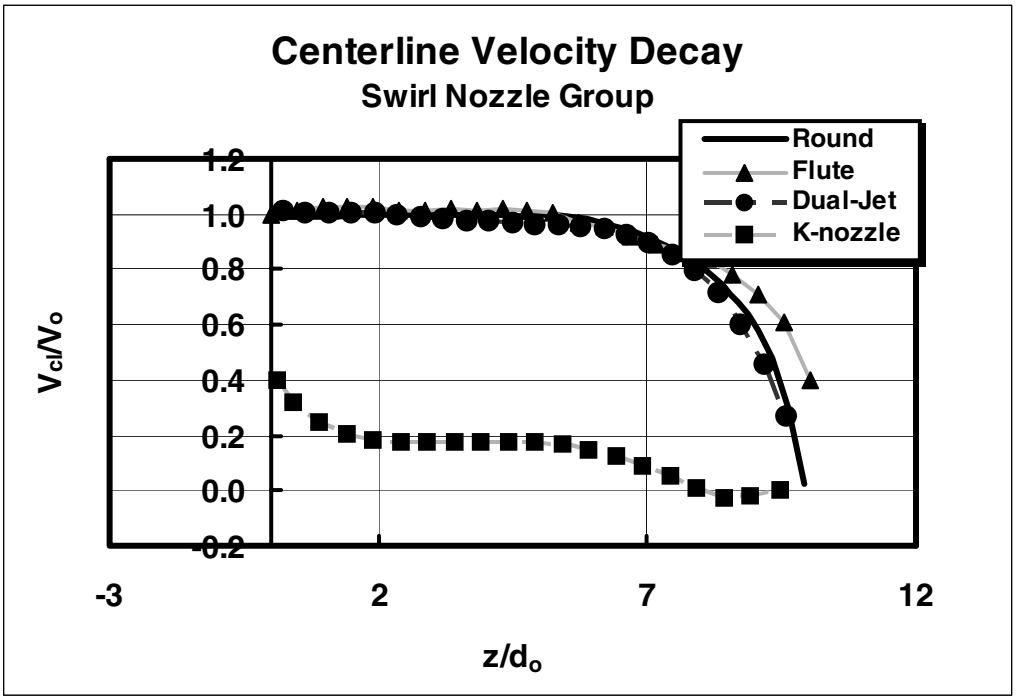

Figure 21 – Axial Velocity Decay – Swirl Nozzle Group

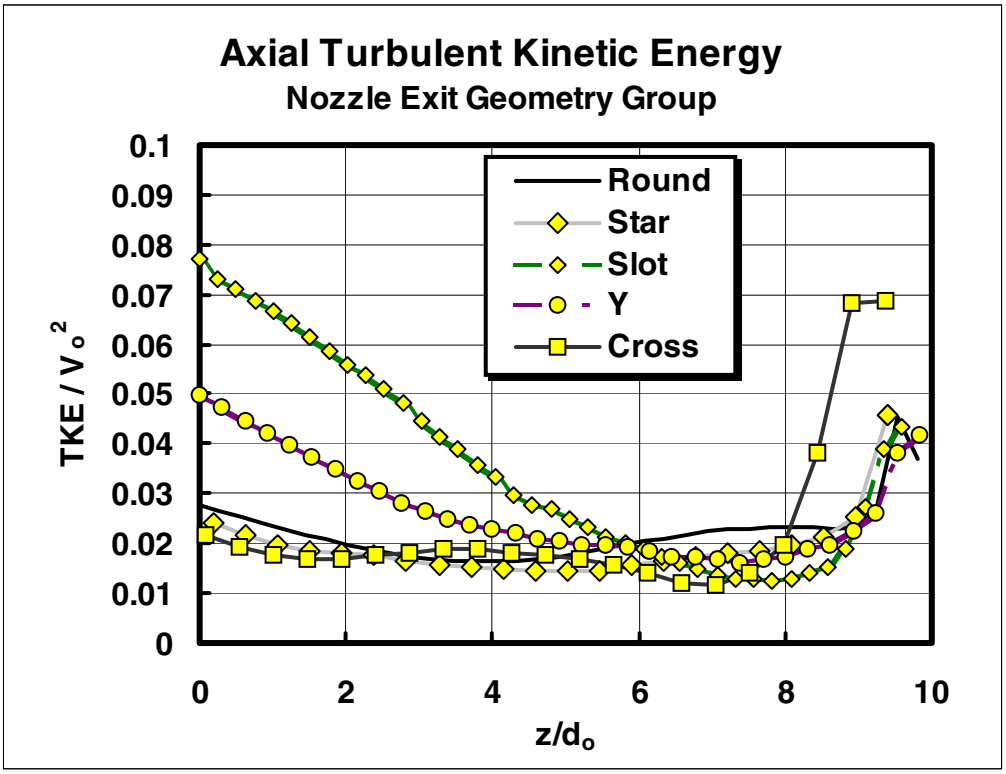

Figure 22 – Axial Turbulent Kinetic Energy – Nozzle Exit Geometry Group

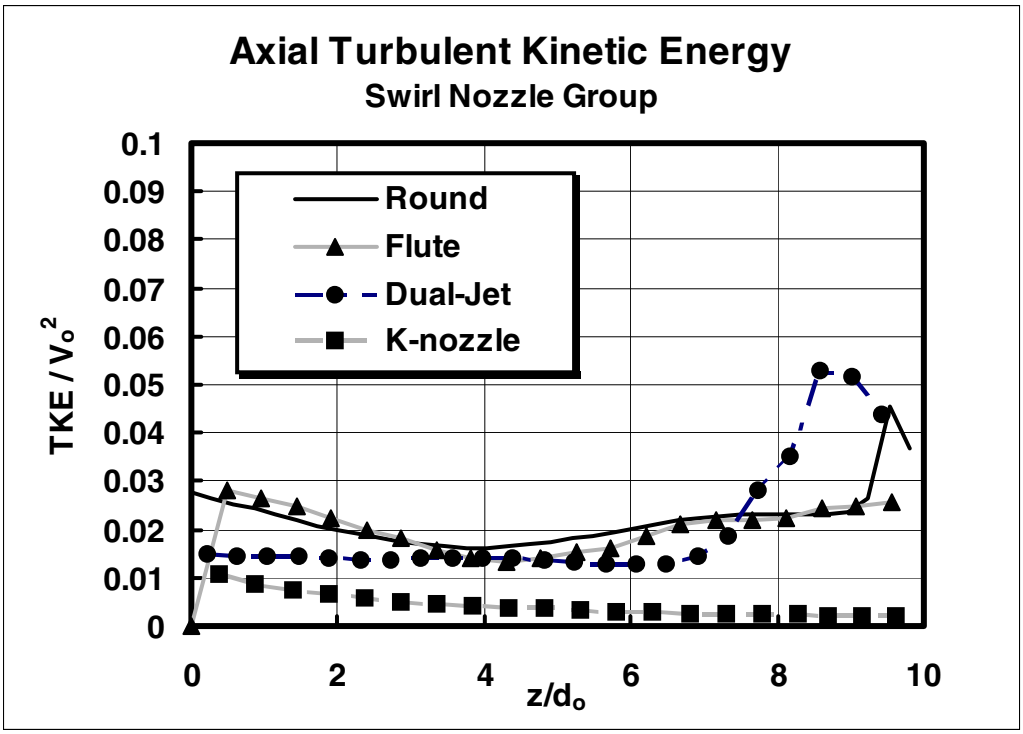

Figure 23 – Axial Turbulent Kinetic Energy – Swirl Nozzle Group

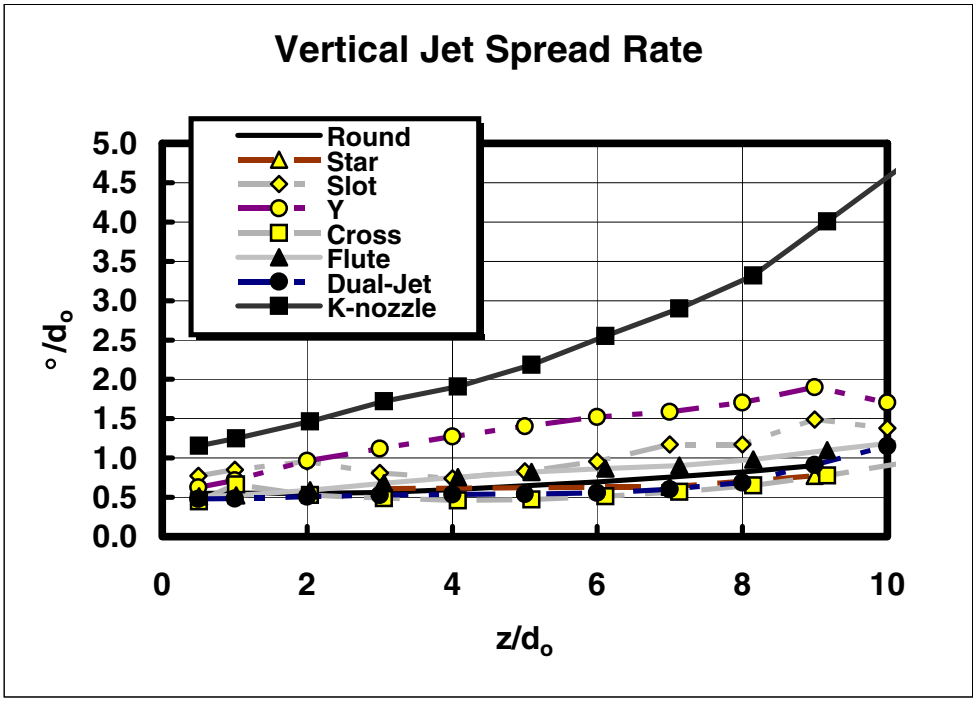

Figure 24 – Jet Spread Rate

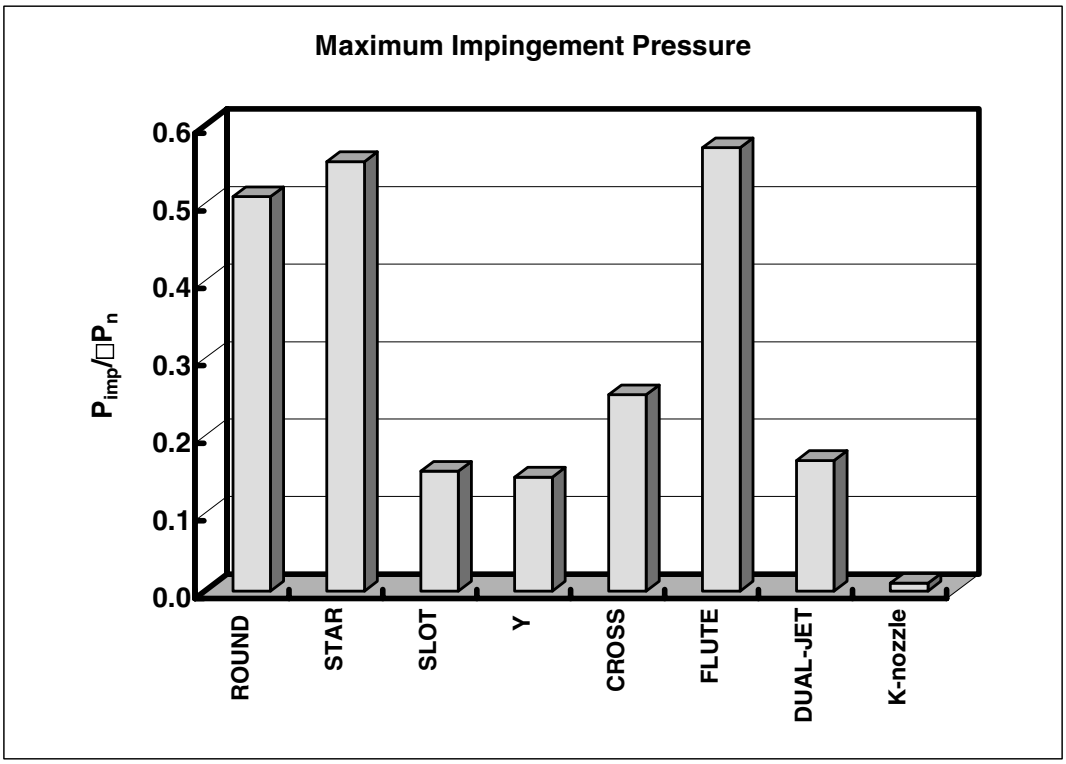

Figure 25 – Impingement Footprint

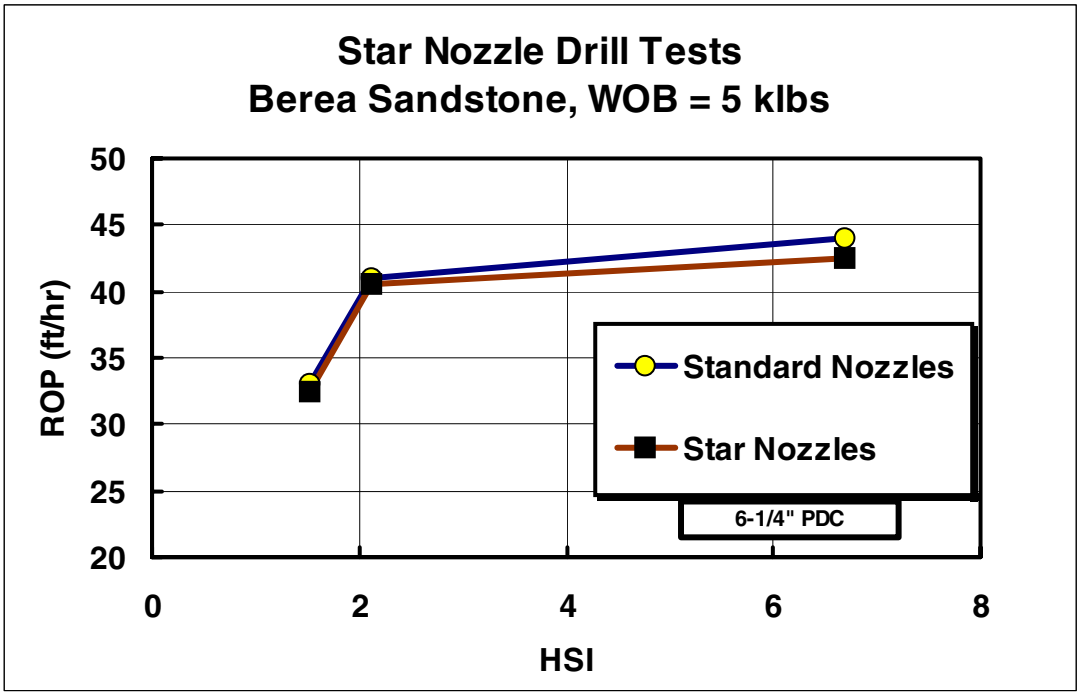

Figure 26 – Drilling Simulator Testing Using the Star Nozzle in Berea Sandstone

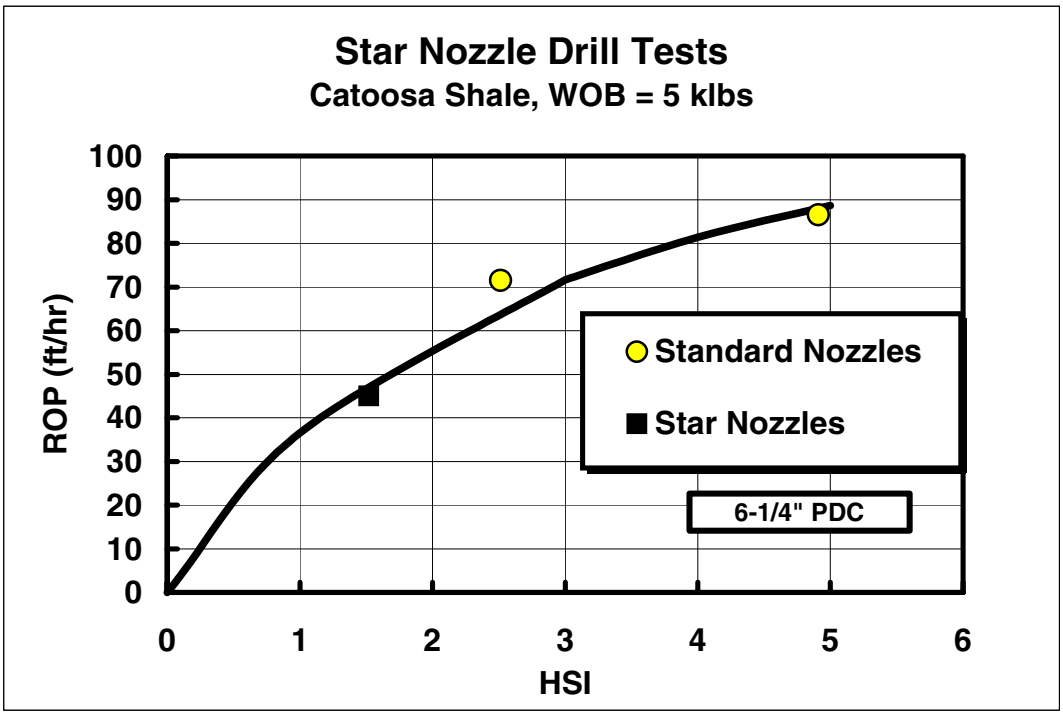

Figure 27 – Drilling Simulator Testing Using the Star Nozzle in Catoosa Shale

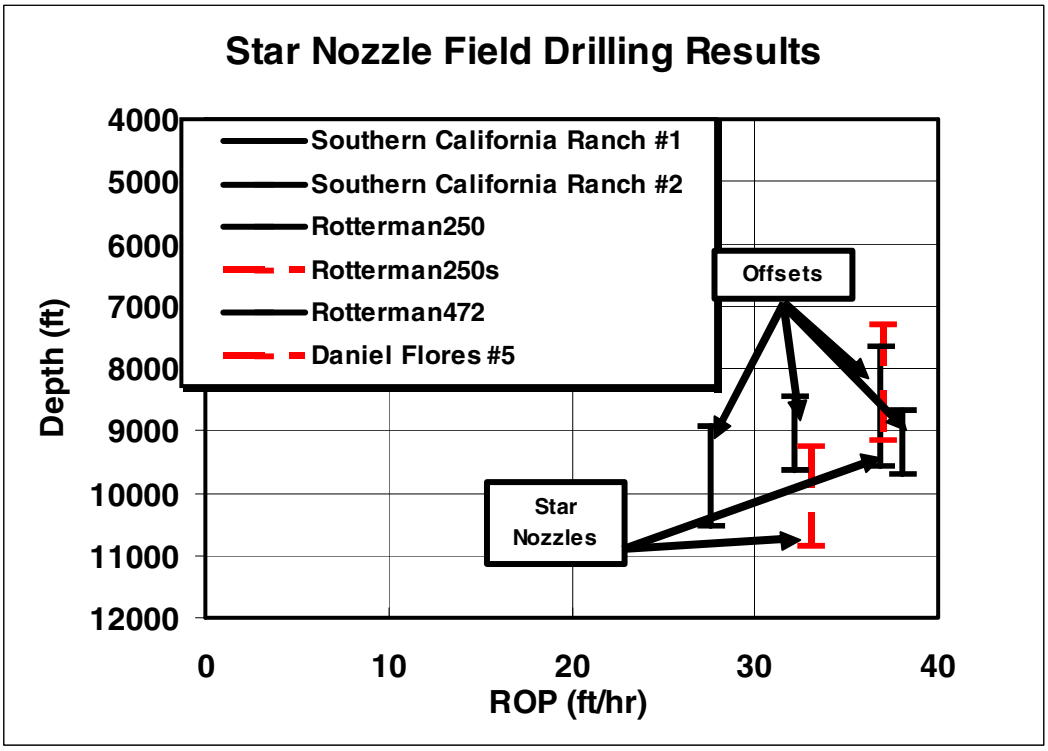

Figure 28 – Field Tests Using the Star Nozzle

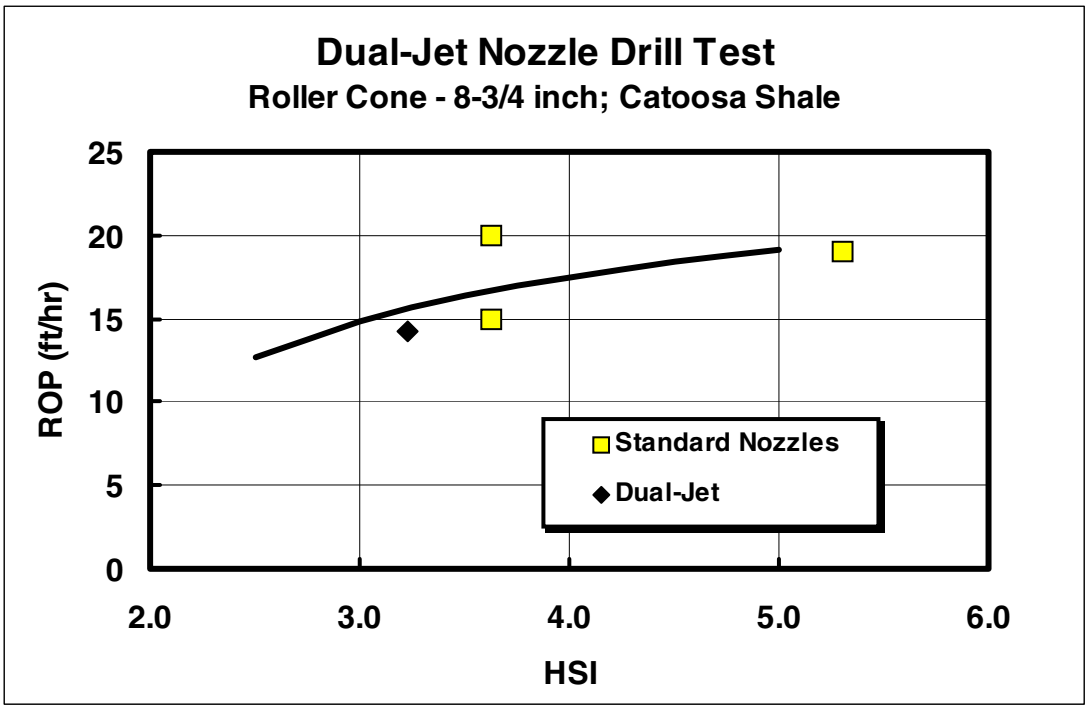

Figure 29 – Dual-Jet Drilling Simulator Results

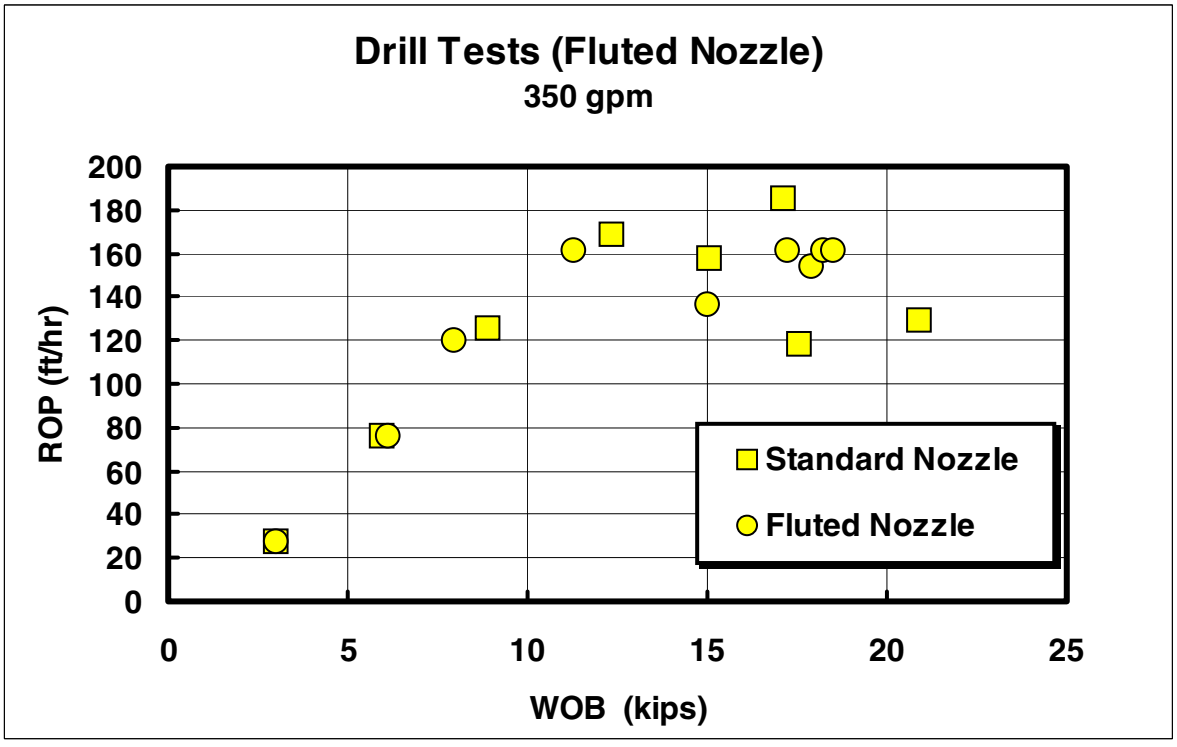

Figure 30 – Drilling Simulator Test Results Using the Fluted Nozzle at 350 gpm